Marine Pollution Bulletin 65 (2012) 425–440

Contents lists available at SciVerse ScienceDirect

Marine Pollution Bulletin

journal homepage: www.elsevier.com/locate/marpolbul

Tidal flushing and wind driven circulation of Ahe atoll lagoon (Tuamotu Archipelago, French Polynesia) from *in situ* observations and numerical modelling

F. Dumas [a,*], R. Le Gendre [d,1], Y. Thomas [c], S. Andréfouët [b]

[a] *Ifremer, DYNECO/PHYSED, BP 70, 29280 Plouzané, France*
[b] *IRD, UR 227 CoRéUs, BP A5, 98848 Nouméa Cedex, New Caledonia*
[c] *Ifremer, DPFOM LPI, Presqu'île du Vivier, 29840 Argenton, France*
[d] *Ifremer, LERN, avenue Général de Gaulle, 14520 Port-en-Bessin*

ARTICLE INFO

Keywords:
Lagoon circulation
French Polynesia
Residence time
Connectivity
MARS3D
Aquaculture

ABSTRACT

Hydrodynamic functioning and water circulation of the semi-closed deep lagoon of Ahe atoll (Tuamotu Archipelago, French Polynesia) were investigated using 1 year of field data and a 3D hydrodynamical model. Tidal amplitude averaged less than 30 cm, but tide generated very strong currents (2 m s^{-1}) in the pass, creating a jet-like circulation that partitioned the lagoon into three residual circulation cells. The pass entirely flushed excess water brought by waves-induced radiation stress. Circulation patterns were computed for climatological meteorological conditions and summarized with stream function and flushing time. Lagoon hydrodynamics and general overturning circulation was driven by wind. Renewal time was 250 days, whereas the e-flushing time yielded a lagoon-wide 80-days average. Tide-driven flush through the pass and wind-driven overturning circulation designate Ahe as a wind-driven, tidally and weakly wave-flushed deep lagoon. The 3D model allows studying pearl oyster larvae dispersal in both realistic and climatological conditions for aquaculture applications.

1. Introduction

Pearl oyster aquaculture is a major source of income for French Polynesia and Cook Islands, and is gaining increasing momentum in different Pacific Island countries. The beautiful black pearls, produced mostly in atoll lagoons, have been the main source of incomes for French Polynesia in the past years, especially between 1995–2003 (Andréfouët et al., 2012a). Tuamotu Archipelago atoll lagoons are essential sources of both spats and adult *Pinctada margaritifera* oysters due to their natural and imported large stocks and their adequate environment for oysters reproduction and growth. An adequate environment is primarily characterized by its bio-physical regime dependant on temperature, water renewal time, and planktonic food availability, both in quality and quantity. The bio-physical regime of the lagoon is largely dependent on the hydrodynamic regime of the lagoon, which is itself dependent on the atoll geomorphology and the atmospheric and oceanic forcing on the atoll boundaries (Andréfouët et al., 2006).

Atolls have different morphologies. Their general saucer-shape lagoon morphology is bounded by a rim which can be completely closed by a continuous emerged rim, or very open to the ocean with continuous submerged reef flats. Open atolls have wide reef flats along most of the perimeter of the atoll, draining waters from the ocean towards the lagoon when waves break along the rim crest. Accordingly, Callaghan et al. (2006) have described wave-driven lagoon-scale processes of flushing in Manihiki and Rakahanga Atolls (Cook Islands). A semi-closed atoll will have few of these reef flats, called also *hoa*, compared to an open atoll. Sometimes, these openings make no more than few tens of meters for an entire atoll. These closed and semi-closed atolls are typical of Tuamotu Archipelago, where they are more frequent than elsewhere.

In addition to the amount of reef flats, atolls may have one or several deep passages allowing water transfer that are driven by local tide cycles. Pugh (1979) provided a simple model of tidal energy dissipation within the deep passage of Aldabra Atoll (Seychelles) and showed that tidal energy dissipation was critically linked to tidal range, lagoon areas and depth of the channel. This induced an attenuated and slightly delayed tide cycle in the lagoon compared to the ocean. In the past, Tuamotu atolls have been ranked according to the number of passes (Salvat, 2009), but this descriptive view is fonctionnaly limited. More functional typologies have been proposed, that relate geomorphology, water renewal mechanisms, and hydrobiological regime (Delesalle and Sournia, 1992; Dufour et al., 2001; Andréfouët et al., 2001).

Atoll water renewal characteristics have been defined and measured in different manners. Andréfouët et al. (2001) based their estimation of a renewal time with a lagoon-scale index dependant on geomorphology and wave-driven flows across the rim openings

* Corresponding author. Tel.: +33 298224676; fax: +33 298224864.
E-mail address: fdumas@ifremer.fr (F. Dumas).
[1] Ifremer, Dyneco, BP 70, 29280 Plouzané, France.

0025-326X/$ - see front matter © 2012 Elsevier Ltd. All rights reserved.
http://dx.doi.org/10.1016/j.marpolbul.2012.05.041

(reef flats and passes). In contrast, Tartinville et al. (1997) characterized for Mururoa atoll an intra-lagoon, spatially-explicit, residence time thanks to field observations and numerical modelling. They also provided a sensitivity analysis of this residence time to various physical forcing variables like wind, waves, tide and stratification. As pointed out by Andréfouët et al. (2006), to be useful for pearl oyster aquaculture management, a lagoon-scale hydrobiological approach is not satisfactory, and a fine-scale intra-lagoon characterization is necessary. To achieve a proper intra-lagoon spatially-explicit hydrobiological characterization, three-dimensional (3D) hydrodynamic numerical models are the tools of choice. They require proper calibration and validation and come with their own limitations, but they allow hypothesis-testing and measuring sensitivity to different forcing factors.

In order to contribute to the management of the pearl oyster aquaculture in Ahe atoll, we used *in situ* measurements and numerical models to characterize the exchanges between the lagoon and the ocean and the main regimes of lagoonal water circulation. In this paper we present the pilot study site, Ahe atoll, with its semi-closed lagoon. Then, we present the suite of *in situ* measurements used to calibrate and validate the model. The various hydrodynamic patterns observed in the hoa, the pass and within the lagoon water body are detailed, as well as the exchanges across the atoll rim and the dynamic response of the sea level. Sensitivity to waves, wind and tidal conditions are discussed. Model outputs are compared to *in situ* measurements throughout. Afterwards, the model is used to characterize the lagoon circulation and map the lagoon e-flushing time. Ahe lagoon hydrodynamic functioning is then discussed, especially in the light of other lagoons described in the literature.

2. Materials and methods

2.1. Study site

Ahe atoll is located in the north-western part of the Tuamotu Archipelago (14°29′S–146°18′W), about 500 km north-east from Tahiti (Fig. 1a). The lagoon is a 142 km^2 deep water body (Fig. 1b) with an average depth of 41 m, and contains numerous pinnacles rising to the surface. The volume of the inner water body is 5.9×10^9 m^3. A detailed lagoon-wide acoustic bathymetric survey revealed that the deeper areas are made of honeycomb-like

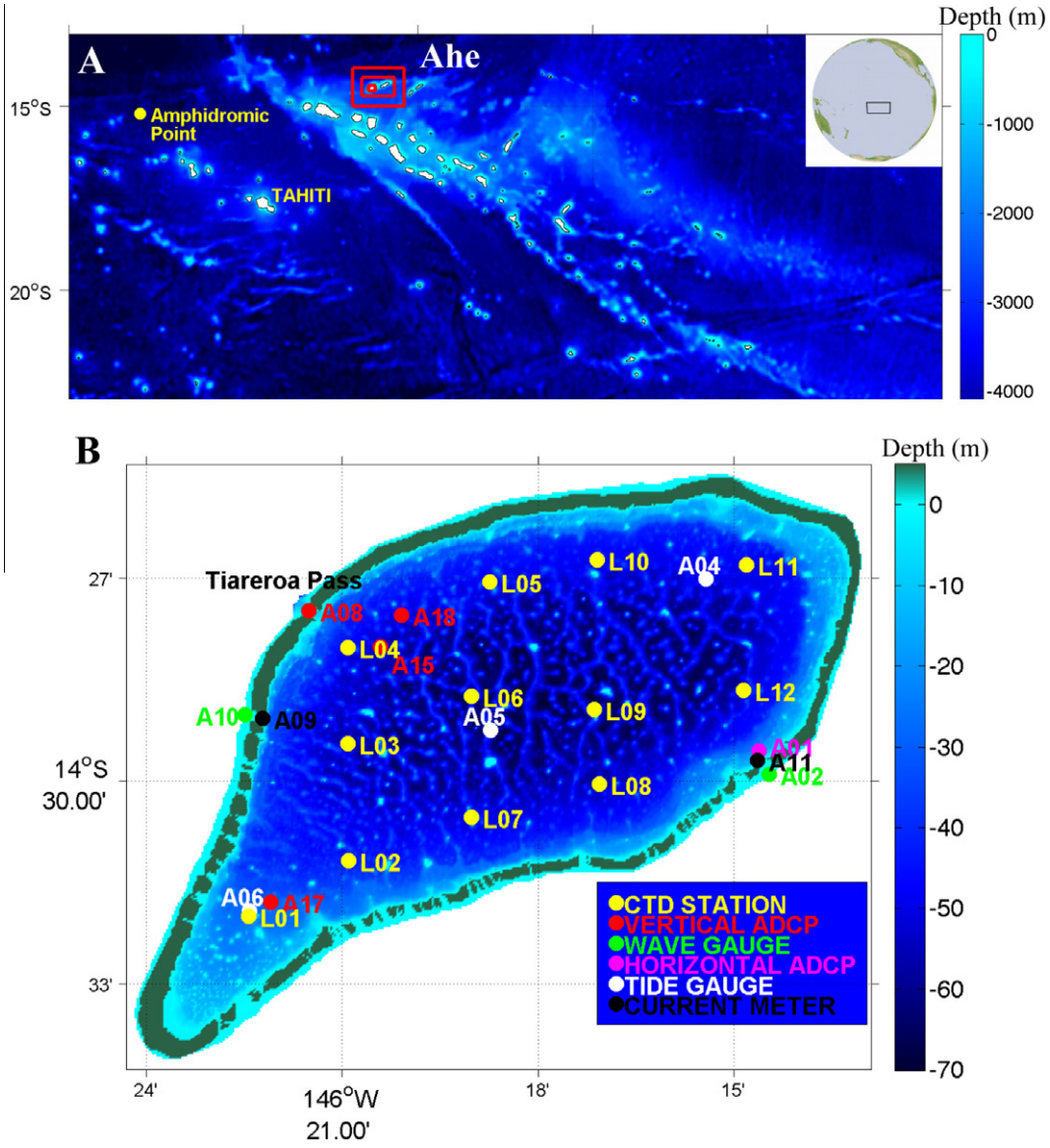

Fig. 1. (A) Map of French Polynesia islands. The extent of this frame is the same as the coarse computational domain. Nested ranks are also shown. (B) Bathymetry of Ahe atoll and locations of the sampling stations, per instrument type (see Table 2).

Table 1
Instrument deployment schedule (date are DD/MM/YY).

	Leg 1	Leg 2	Leg 3	Leg 4	Leg 5
Begins	02/12/08	09/02/09	24/04/09	28/06/09	28/09/09
Ends	08/02/09	24/04/09	28/06/09	28/09/09	07/11/09

cellular structures probably of karstic origin, in which individual basins reach up to 70 m deep.

The lagoon is an almost closed water body connected to the open ocean through a 11-meter deep, 200-meter wide pass. The *Tiareroa* pass is located on the north-west side of the atoll rim (Fig. 1b). Several very shallow hoa (about 30 cm deep, between 10 and 300-meter wide, with a total cumulated width of 4 km), represent about 5% of the rim perimeter (77 km). Hoa are present on the southern side and on the north-western side of the rim. The northern part of the rim located east from the pass, and most of the eastern part of the rim, are completely closed to water exchanges (Fig. 1b).

The wave regime around Ahe atoll is described by Andréfouët et al. (2012b). Ahe atoll benefits from a sheltered position due to the relative position of nearby atolls. It is very efficiently sheltered from the southern oceanic waves by a series of large southward atolls, and it is also sheltered, although less efficiently, on its east side by Takaroa and Takapoto atoll. North swells generated by northwest Pacific depressions occur from November to March and they hit directly Ahe's northern rim, but wave height in the north of the atoll is typically low with an average wave height around 1.7 m, including the contribution of wind waves. As a result, Ahe is mostly exposed year round to wind waves generated locally by dominant easterly tradewinds, which are stronger from April to October. Andréfouët et al. (2012b) showed that Ahe is exposed to wave height above 2.5 m only a few days per year.

Ocean tidal amplitudes near Ahe atoll are small (around 40 cm) due to its proximity to a M2 amphidromic point (Fig. 1a).

2.2. In situ hydrodynamic measurements

Continuous physical measurements were made during nearly 1 year between December 2008 and early November 2009. *In situ* data acquisition took place during 5 legs of continuous recording, with data downloading and instrument maintenance occurring

Table 2
Description of moored instrument deployments used for this study. See Fig. 1 for locations of stations. SP = sampling period.

Station	Location	Instrument	Depth (m)	Legs deployed	Sampling
A02	14°29.909′S 146°14.466′W	Tide and wave recorder TWR-2050	6.8	1,2,3,4,5	SP waves: 20 min SP tide: 10 min
A04	14°27.086′S 146°15.435′W	Pressure recorder DR-1050	50.5	1,2	SP: 10 s
A05	14°29.326′S 146°18.727′W	Pressure recorder TGR-1050	53.7	1,2,3	SP: 10 s
A06	14°31.989′S 146°22.429′W	Pressure recorder DR-1050	25	1,2,3	SP: 10 s
A08	14°27.488′S 146°21.511′W	ADCP Sentinel (1200 kHz)	17	1	SP: 10 min Bin size: 0.5 m
A09	14°29.077′S 146°22.224′W	Current-meter Aanderaa RCM7	0.8	1,2,3,4,5	SP: 10 min
A10	14°29.024′S 146°22.488′W	Pressure recorder TGR-1050	6.1	1,2,3,4,5	SP: 1 s for leg 1, 2 s for others
A11	14°29.698′S 146°14.639′W	Current-meter Aanderaa RCM7	0.8	3,4,5	SP: 10 min
A15	14°28.021′S 146°20.422′W	ADCP Sentinel (1200 kHz)	22	3	SP: 10 min Bin size: 2 m
A17	14°31.791′S 146°22.092′W	ADCP Sentinel (1200 kHz)	20	4	SP: 20 min Bin size: 2 m
A18	14°27.549′S 146°20.097′W	ADCP Sentinel (1200 kHz)	20	5	SP: 10 min Bin size: 2 m

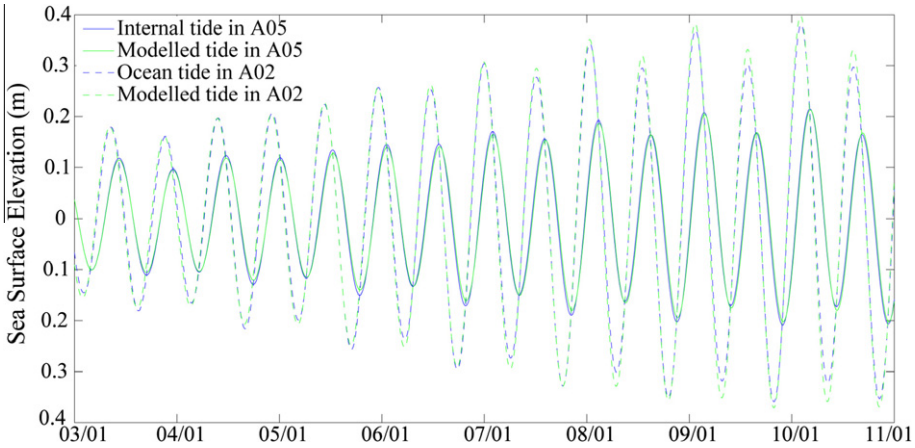

Fig. 2. Half spring-neap tidal cycle (January 2009) of sea surface elevation in A05 (lagoon) and A02 (ocean). Model *versus in situ* data are displayed, but they are in very close agreement and overlap almost perfectly.

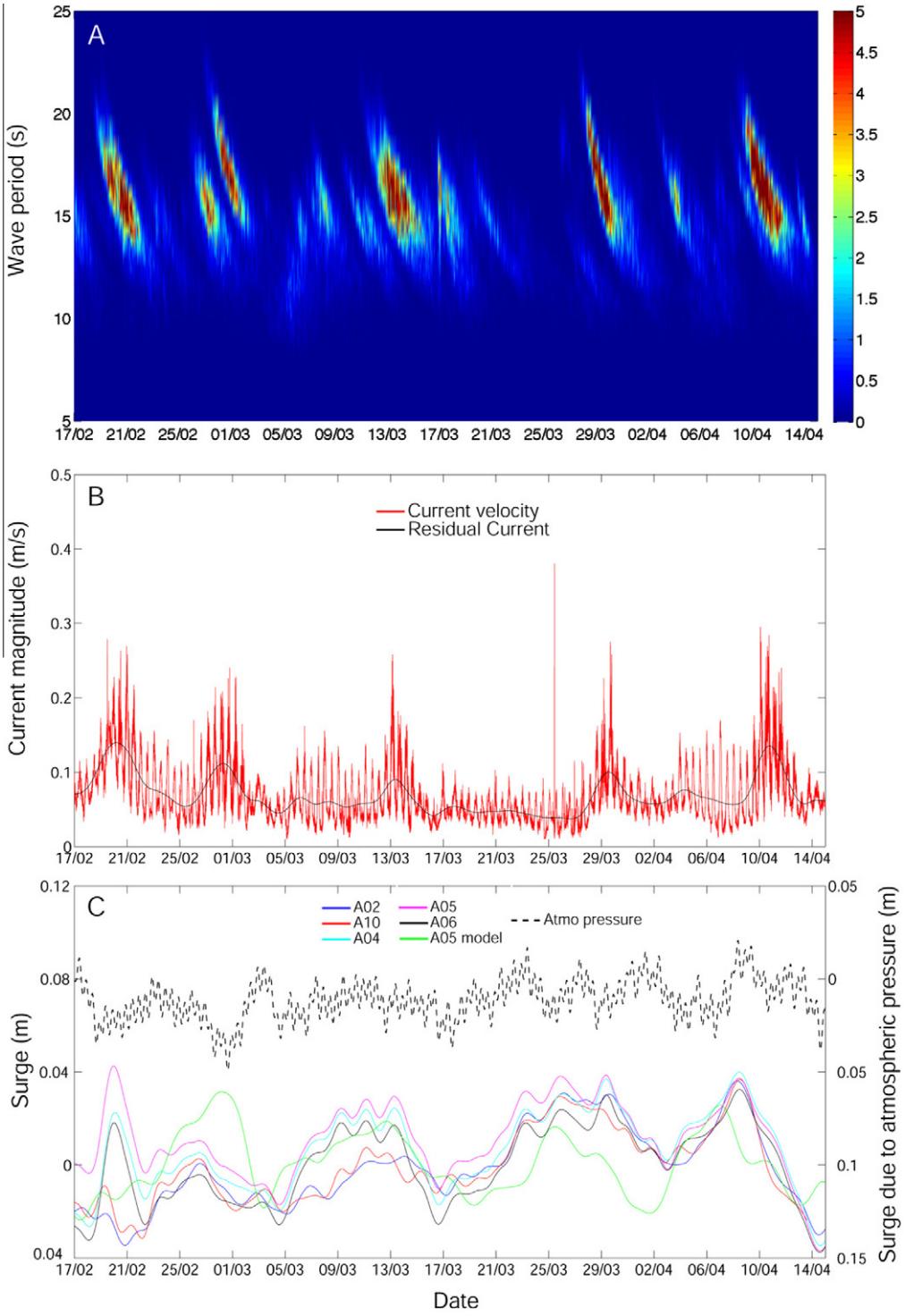

Fig. 3. (A) Forereef wave energy spectra (color bar in $m^2\ Hz^{-1}$) in A10 (in front of the northern hoa, Fig. 1) from mid-February–mid-April 2009. (B) Concurrent instantaneous and tidally filtered currents in A09 (northern hoa). (C) Concurrent de-tided sea surface elevations inside and outside of the lagoon and inverse barometer surge.

every 2 months, at the exception of the last leg which lasted 3 months (Table 1).

The global strategy for data acquisition was to measure in a coordinated fashion the incident waves on the forereef, water levels and tide inside and outside the lagoon, currents through the rim (hoa and pass), and currents in different locations inside the atoll for a better understanding of the circulation. The sampling was designed to assess the co-influences between the processes taking place at the lagoon boundary and inside the lagoon. Table 2 explains the instruments deployment. For each leg, the mooring locations were the same except for the upward-looking 1200 kHz acoustic Doppler current profiler (ADCP, RD Instruments Workhorse Sentinel) which was used in different locations from one leg to another.

Two functional (i.e. always active with flowing waters) hoa were selected and instrumented. One was located on the northwest (Station A09) and one on the southeast side (Station A11). For measuring current velocities, rotor current meters (Aanderaa

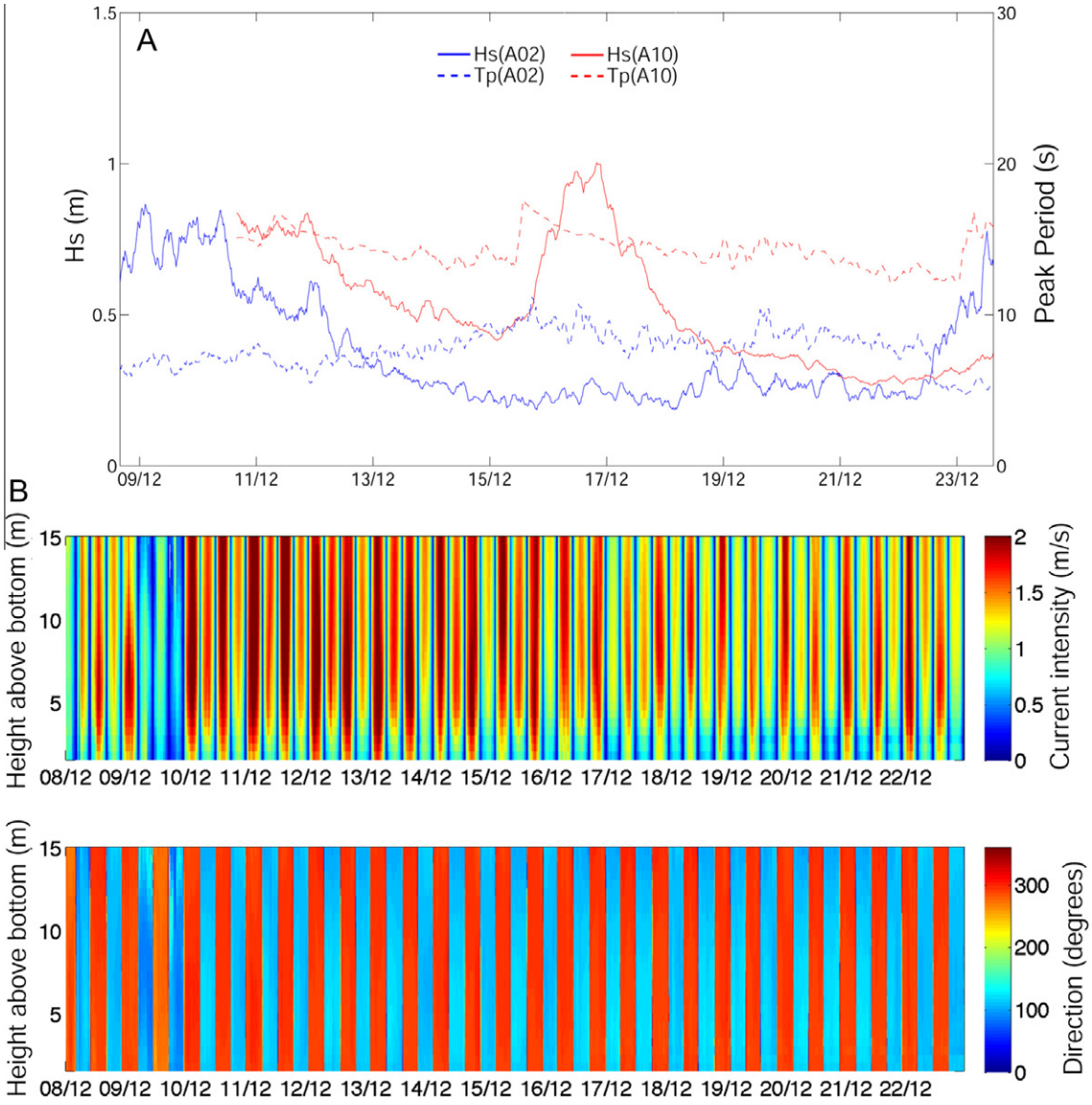

Fig. 4. (A) Significant wave height and peak period in A02 (southern hoa) and A10 (northern hoa) in December 2008. (B) Concurrent vertical profile of instantaneous current intensity and direction from the ADCP in the pass (A08). The current flows outbound around 340° (red), and inward around 120° (blue). (For interpretation of the references to colour in this figure legend, the reader is referred to the web version of this article.)

RCM7) were used, casted in concrete with their blades disassembled. This system measured velocities every 12 s, then stores an average value over a 10 min time step.

The north incident waves as well as sea levels were measured using a pressure recorder (TGR-1050, RBR), moored on the external oceanic forereef slope (Station A10). This sensor sampled pressure every 1 or 2 s. On the south side of the atoll, a tide and wave recorder (TWR-2050, RBR) was also deployed (Station A02). Its sampling period for tide was 10 min. Measurements were the average of 1 min-long acquisition at 2 Hz. Wave data were stored every 20 min using burst lengths of 512 samples at 2 Hz.

For the lagoon tide characterization, three pressure recorders were moored aligned in Ahe longitudinal axis (Stations A04, A05, A06). They recorded pressure data every 10 s.

During the first leg, the vertical Sentinel ADCP was moored in the pass (Station A08) to evaluate the magnitude of the main exchanges between ocean and lagoon. Other lagoon sites were also investigated using additional vertical current profiler in this first leg, and with the Sentinel subsequently. This includes the sector near the pass (with Stations A15 and A18). A location in the south-west of the lagoon (Station A17) was also monitored to study recirculation phenomenon. For all legs, the vertical profiler averaged currents over 250 pings per ensemble. Ensemble interval was generally set to 10 min except for the fourth leg which lasted 1 month longer than the others.

During each field campaign aimed at downloading data and servicing the instruments, hydrologic surveys were carried out to provide profiles of temperature, salinity, oxygen and pH along the water column at Stations L01 to L12 using a multi-parameter profiler CTD Seabird SBE 19 plus.

2.3. Post-processing

The pressure data from the recorder in A10 were transformed to depth data, and converted to surface wave-height data using inverse Fourier transforms. The processing of de-tided signals (levels in Fig. 2, currents in Fig. 3 and flow in Fig. 4) has been performed using Demerliac filter (Demerliac, 1974). This filter is specifically

designed to remove tidal harmonic constituents from any signal using a 72 hour window. For level analysis, in order to have all the signals centered on the same vertical referential, mean value of depth over the entire duration of the time series was subtracted from instantaneous values. Tide harmonic analysis was made with the T_tide toolbox (Pawlowicz et al., 2002).

2.4. Numerical modelling

The MARS3D numerical model used here has been described in detail by Lazure and Dumas (2008). In short, it is a standard model based on classical assumptions (Boussinesq approximation, hydrostatic balance assumed) that leads to a set of equations that is solved using finite difference techniques in a sigma coordinate framework. The resolution is based on mode splitting as in Blumberg and Mellor (1987). The turbulent eddy diffusivity and viscosity are assessed using the Gaspar (1990)'s turbulence closure.

To model Ahe lagoon, four different levels of nesting were required (Fig. 1a). The first three levels are bi-dimensional horizontal approximation. They describe the open boundary conditions of the atoll, including astronomical and meteorological tides. The wider model is forced by a sea level signal harmonically composed from FES2004 (Lyard et al., 2006), accounting for an inverse barometric correction estimated from the NCEP Global Data Assimilation System (GDAS) pressure field. The barotropic mode (sea surface height and mean vertical velocity) along the open marine boundaries is thus provided by the immediately wider model of the embedment.

The bathymetry at the nodes of the grids were obtained from various sources: ETOPO1 bathymetry grid was used for the large scale. For the deep atoll slopes, we digitized nautical charts from the French Oceanographic and Hydrographic Service (SHOM). Inside the lagoon, bathymetry (Fig. 1a) has been mapped using a single beam acoustic sensor on east–west oriented tracks spaced 50 m apart. The pass and some large pinnacles were surveyed following a finer mesh of about 10 m resolution.

The detailed inner hydrodynamic model has a spatial resolution of 100 m. It encompasses entirely the lagoon, the rim and most of the external slope. On the vertical axis, 23 sigma layers are distributed to represent both the bottom and the surface boundary layers.

The atmospheric forcings were computed thanks to bulk formulae following Luyten and de Mulder (1992). These formulae require wind velocity at 10 m, pressure at the sea level, relative humidity and air temperature at 2 m, and finally fractional cloud cover. These meteorological conditions were obtained from a Meteo France weather station located at the Takaroa station (14°28.460′S–146°2.285′W). Hourly data of wind intensity and direction, pressure at sea level, temperature and cloud cover were gathered, and given the Ahe-Takaroa distance (150 km) and lack of any orographic effects in atolls, Takaroa data were considered valid for Ahe. At the scale of the process examined here, we considered that meteorological conditions could be taken homogeneous over the modelled area. An alternative choice would be to use GDAS analysis, but the 50 km spatial resolution does not provide a significant enhancement compared to the Takaroa meteo station data. Moreover, GDAS temporal (6 h) were far worse than local data.

2.5. The e-flushing time

There are various ways of investigating the retention capability of a semi enclosed water body like Ahe. A useful bulk variable is the renewal time. It has been defined as the ratio of the total volume of the water mass to the incoming flow that flushes it. This gives an integrated measurement at lagoon-scale. However, the retention capability varies in space. It is inherently constrained by the morphology of the basin (independent of time) but it also depends on dynamic time-dependent forcing factors such as tide, wind and flow forced by waves. To refine the notions of retention that have been introduced by Thomas et al. (2012a,b) for larval dispersal and spat collecting, we introduce hereafter the e-flushing time.

E-flushing time aims to map the most favourable retention areas, and their variability with respect to forcing. It helps understanding the numerical experiences shown by Thomas et al. (2012,b). The e-flushing time is defined as follows: at a given location, it is the time needed to decrease a concentration of tracers (e.g., larvae) by a factor $e = 2.718$. Thus the concentration is about 60% lower than the initial concentrations. The e-flushing time is estimated with the model, using passive tracer homogeneously distributed in the lagoon water body at the initial time. Initial concentrations are fixed, equal to 1 unity.m^{-3}. Every water flux entering the lagoon (either by the main pass or the hoa) has a null concentration. The transport equation is then integrated along with dynamical evolution of the flow to update the concentrations and the current e-flushing time.

3. Results

3.1. Tide

The tidal spectra was mostly made of components that are in the tide-generating potential. Accordingly, it is of oceanic type because non linear effects giving birth to interaction with waves are very weak. The harmonic constituents at Station A02 are provided in Table 3. The M2 amplitude was 23 cm and the sum of the main semi-diurnal components reached 34 cm whereas the main diurnal components reached 4 cm, thus slightly less than a tenth of the semi-diurnal. This defined a mostly semi-diurnal with diurnal irregularities tidal regime. The mean tidal range was around 50 cm, decreasing to 31 cm during neap tide and increasing up to 73 cm in spring tide. As modelled by Pugh (1979), tidal energy was severely dissipated by the Tiareroa pass, thus the lagoon inner tide amplitude was limited to 20 cm during neap tide and 32 cm during spring tide. Associated to this damping, a significant delay between the inner and outer tide was observed corresponding to a M2 phase of 54°, or in other words almost a two hours lag. The three tidal gauges (A04, A05, A06, Fig. 1b) within the lagoon showed that at least the M2 component is homogeneous throughout the lagoon, although phase shifts of 0.2° (i.e. 25 s) between A04 and A06 could be calculated. No differences greater than a millimeter in amplitude were detected between the three lagoon sites.

Fig. 2 compares the pure astronomical tide reconstructed from the five main components extracted from gauges A02 (ocean) and A05 (central lagoon) and the model at the same locations. Except the five main components M2, S2, N2, O1 and K1, others have an amplitude of about 1 mm or less, and thus they were neglected afterwards. Models and observations are in good agree-

Table 3
Comparison of measured and modeled tidal harmonic constituents between open ocean in Station A02 and lagoonal tide in Station A05.

Harmonic constituent	A02 H (m)	A02 model H (m)	A02 G (°)	A02 model G (°)	A05 H (m)	A05 model H (m)	A05 G (°)	A05 model G (°)
M2	0.236	0.249	98.29	93.72	0.139	0.139	154.04	156.14
S2	0.065	0.075	57.46	63.23	0.032	0.034	123.63	134.87
N2	0.049	0.049	77.04	76.33	0.024	0.023	140.00	143.63
K1	0.029	0.022	93.46	87.36	0.020	0.017	137.48	135.97
O1	0.012	0.012	32.00	10.51	0.009	0.009	69.60	59.53

ment. Outside the lagoon (A02), Table 3 shows that the amplitudes differ from less than 1.5 cm at most, whereas the phase lag (except curiously for O1, the weakest wave) is of the order of 5°, representing a 10-min lag for semi-diurnal components. This slight discrepancy between model and observations is explained by the use of FES2004 and the bathymetry ETOPO1. Within the lagoon, observations and model fitted perfectly (Fig. 2), with time delay less than 15 min and amplitude difference which are lower than 2 cm. The good agreement suggests that our bottom parameterization was sufficient (bottom drag coefficient, which is based on a log law approximation, and roughness set to 3.5 mm; lateral friction was accounted for in the bottom friction parameterisation and the sigma vertical framework) and that the influence of the pass due to its geometry was also correctly represented at the 100 m spatial resolution used here.

3.2. Waves, current in hoa, and lagoon surge

This section analyses the variation of sea surface elevation in the lagoon, after filtering out the astronomical tide. An example of sequence is shown for February–April 2009, for the different stations (Fig. 3c). In relation to oceanic surface and lagoon surface elevation, the distribution of wave energy measured on the north side of the rim according to the wave period (Fig. 3a) shows the effect of incoming waves generated in higher northern latitudes. The dispersion effect is visible on the spectra Fig. 3a as the longer wave arrives first, in agreement with the dispersion relation of linear Airy waves in infinite depth, which implies that longer waves propagate faster. In Fig. 3, the period of the swell reaching Ahe varied from 19 to 13 s, and its significant wave height reached up to 1.40 m (observed on the 5th of January – not shown). Current velocities measured at Station A09 in the northern hoa during the same period are shown Fig. 3b. The current intensity appeared very well correlated with the sea state observed at Station A10 in the ocean. The black curve Fig. 3b is the intensity of the current filtered by Demerliac filter to remove tide effects. The maxima fit very well with wave trains observed outside the atoll at point A10. The instantaneous de-tided current may be of the order of 28 cm s^{-1} when waves are present, and it peaked at 30 cm s^{-1} the 10th of April 2009 in Fig. 3. Strongest velocities were measured at 38 cm s^{-1} the 16th September 2009 (not shown). Tidal influence was evident too in the hoa unfiltered signal (red curve, Fig. 3b). The current in the hoa peaked at high tide and was minimum at low tide. Even without significant waves from the north, the hoa remained active with a light residual current at few cm s^{-1} (Fig. 3b). As the cumulated length of the few hoa on the northern

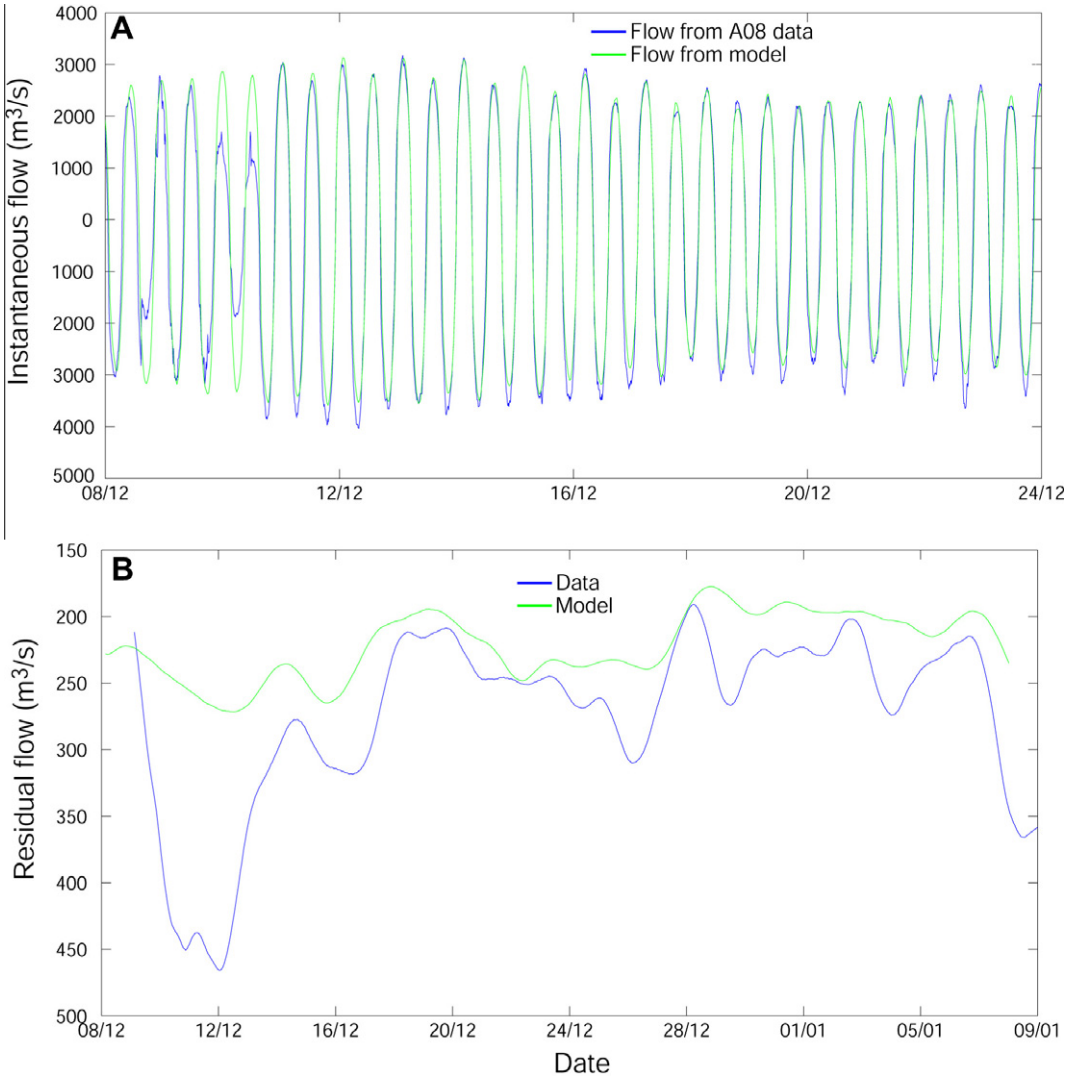

Fig. 5. (A) Instantaneous flow through the pass section deduced from the observations and simulated by the model, in December 2008. (B) Residual flow through the pass section (A08) from the observations and the model, during 1 month.

side of the rim is nearly 500 m, assuming all hoa work in the same manner, the cumulated water flux entering the atoll by the northern side is about 50 $m^3 s^{-1}$.

Time series of current from the southern hoa (Station A11) show the same behaviour as the north hoa, with a modulation with respect to the tidal signal and a good correlation with the significant wave height measured outside the rim in front of the hoa (Station A2). A commonly observed sea state (Hs = 1.5 m and Tm = 8 s) generates tidally filtered currents of 15 cm s^{-1} within the southern hoa. The strongest currents over the period of the survey occurred on the 4th of October 2009. The tidally filtered currents peaked to 50 cm s^{-1}, during a time where significant wave height and peak period estimated by WAVEWATCH III model (Andréfouët et al., 2012b) were 2.5 m and 8 s respectively.

Given the low variability and low velocity of hoa current observed during the entire survey both in the north and south sectors, the hoa parameterisation has been simplified in the model. Velocity across all hoa has been tuned permanently to a mean value of 10 cm s^{-1}, which was the average value observed over the entire observation period (1 year). Under the assumption that all southern hoa work in the same manner at the same time, this average value induces a mean inflow during a half tidal cycle of 103 $m^3 s^{-1}$. This is ten to twenty times smaller (i.e. 1340 to 2010 $m^3 s^{-1}$) than the flux exchanged through the main pass during the same time by the tide alone as previously evidenced. If we consider that the volume extracted through the pass during half a tidal cycle is not the same as the one re-entering during the next half-tidal cycle, it appears that over the year, on average, the contribution of the hoa to the flush was weak, and an order of magnitude lower to tidal flushing. During short energetic events when wave height was above 2.5 m, the velocity in the hoa can reach about 50 cm s^{-1} (e.g., 4th of October 2009). In that case, hoa contribution was only two to four times weaker than the tidal flushing, and it could be considered significant compared to pass flushing.

During the entire survey (December 2008–November 2009), the maximum lagoon surge amplitude observed was only 6 cm, observed for example the 8th February 2009 (Fig. 3c). All gauges (A04, A05, A06) generally reacted in the same manner, but some difference occurred the 20th February with a 2.5 cm difference between A06 and A05, and again on the 13th and the 25th of March. This weak difference and the consistent reaction of the three gauges show that water level variations are rather homogeneous lagoon-wide. Fig. 3c shows that the mean sea level computed by the model is in agreement with the observations (i.e. −4 cm to 4 cm). A clear signal, with a period of a fortnight, is visible in the observation and is well reproduced by the model. The largest discrepancy occurred on the 21st of February 2009 when the signal observed in northern hoa (15 cm s^{-1}) was stronger than the signal forced into the model. The resulting surge was thus underestimated by the model at this date. In addition, on the 1st of March 2009, the model reacted more rapidly to a shift in the atmospheric pressure than what was observed.

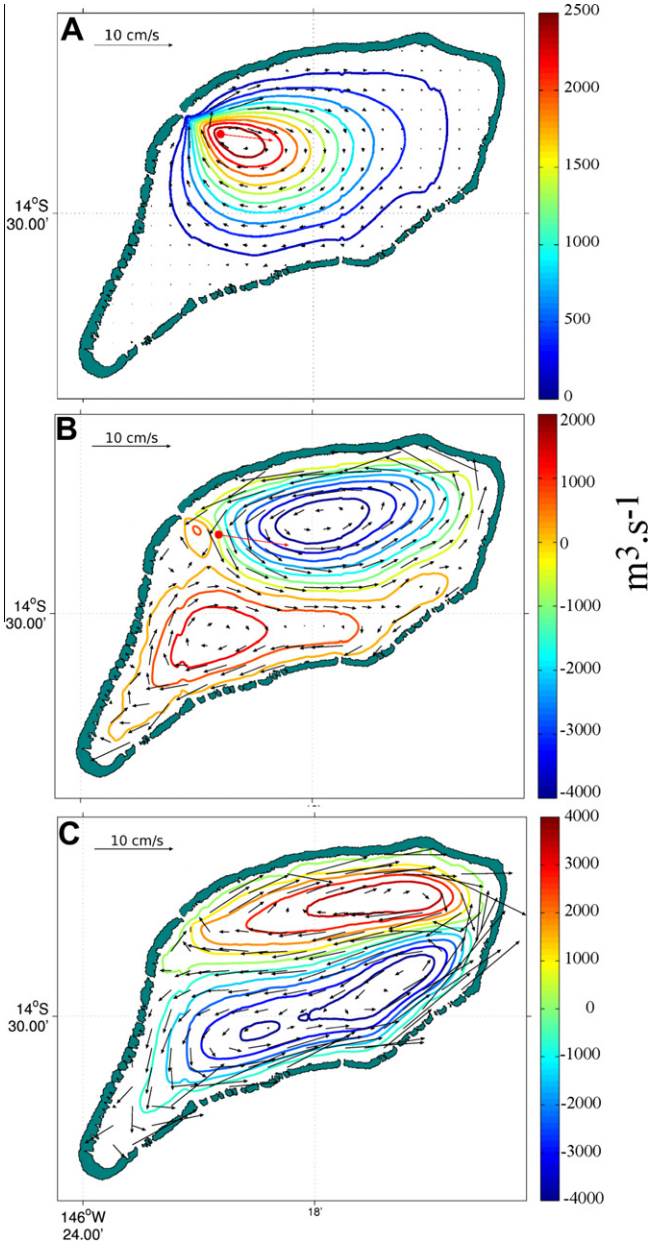

Fig. 6. (A) Barotropic stream function (contours in $m^3 s^{-1}$. Note that scales are different per panel) and barotropic current fields of the tidally filtered, modelled, current field (BSF). The flow is driven by tide alone. Estimates from ADCP measurements are shown by the red arrow (B) BSF with the flow driven by tide and stationary average tradewinds (107° – 8 m s^{-1}). (C) BSF with the flow driven by tide and stationary western winds (270° – 8 m s^{-1}). (For interpretation of the references to colour in this figure legend, the reader is referred to the web version of this article.)

3.3. Exchanges through the pass

The instantaneous current profiles measured in the middle of the pass (Station A08, first leg, see Table 1) showed that the current was essentially bidirectional (340° during ebb tide and 120° during flood tide) and tightly coupled to tide variations (Fig. 4). The current is thus clearly semi-diurnal. Over the period (a fortnight), tidal reverse was always clearly visible even the 10th of December 2008 when the flood was severely dampened. The tidal reverse always happened in less than ten minutes (Fig. 4b). The intensity of the current ranged from 1.2 m s^{-1} (neap tide) to 2.5 m s^{-1} (spring tide), except during the 10th December event.

The vertical profiles showed the classical decrease expected next to the bottom due to the friction. The thickness of this bottom boundary layer was about 4 m. Above this boundary layer, the profile was usually rather homogeneous up to the surface, even if maximum regularly occurred (9th, 18th, 21st) 6 m above the bottom. Also, the current was systematically stronger during ebb tide than flood tide. The direction was almost homogeneous along the vertical axis: only a slight veering was noticeable during flood from 140° at the bottom to 120° at the surface.

The flow through the pass has been estimated using the ADCP current profiles and a bathymetric transect passing through the ADCP mooring. The model used to build an integrated flow through

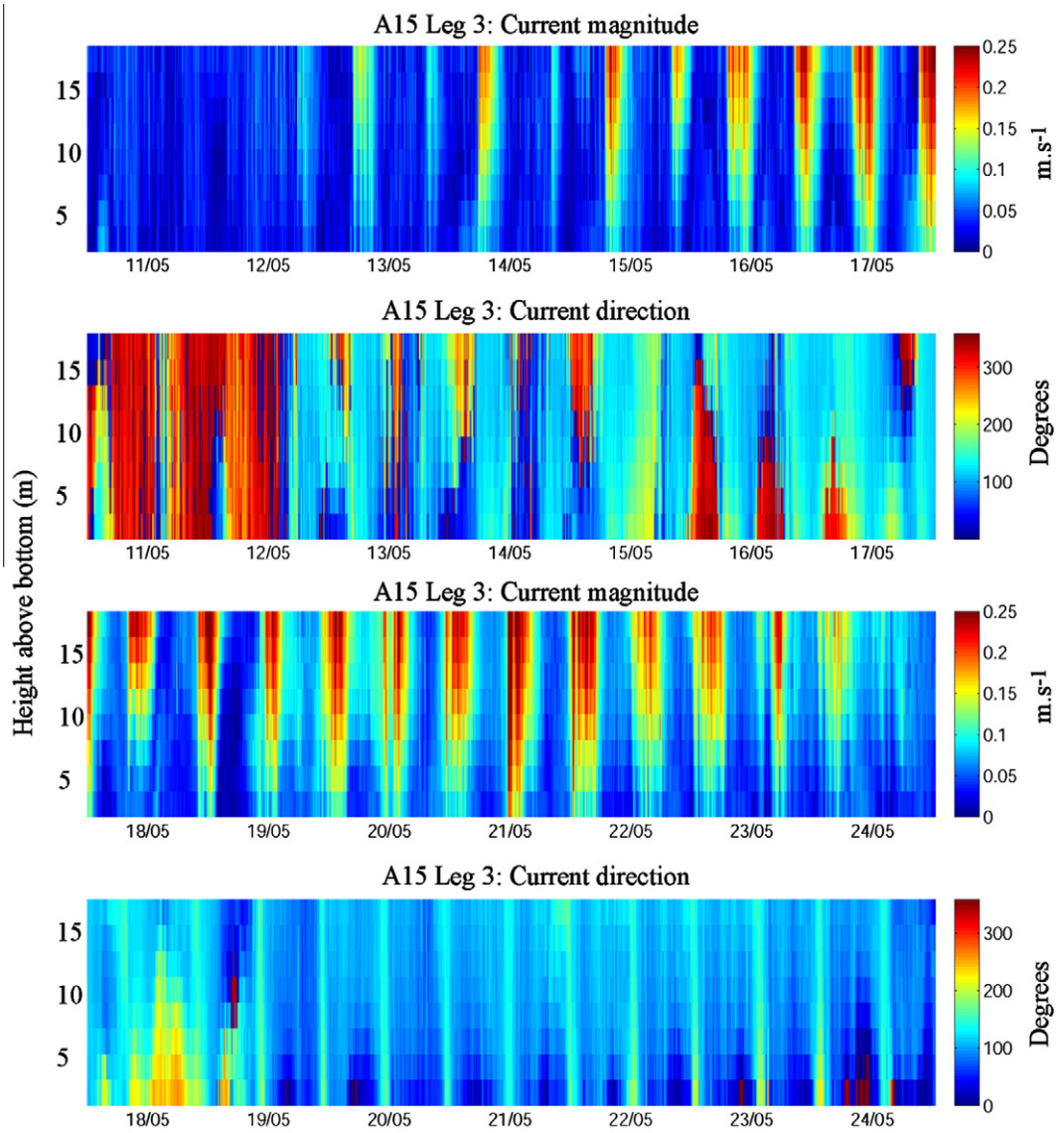

Fig. 7. Vertical profiles of currents observed at location A15.

the whole section of the pass relied on the assumption that the main equilibrium of the forces that drive the flow at any point of the section is between external pressure gradient and friction, thus giving :

$$\frac{\partial \zeta}{\partial n} = \frac{\overline{u}^2}{\mathrm{St}^2 H^{4/3}}$$

if the bottom friction is parameterised thanks to Strikler (St) coefficient, $\overline{u}$ is the vertically averaged current, ζ is the sea surface elevation, H is the total water depth. This equation at Station A08 provided the sea surface slope. Assuming the surface slope is constant along the transect and knowing H, we deduce $\overline{u}$ along the section, and finally integrate the flow through the pass (Fig. 5a). Instantaneous flows (Fig. 5a) were clearly semi-diurnal, varying from 2000 $m^3\ s^{-1}$ (neap tide) to 3000 $m^3\ s^{-1}$ (spring tide). The total amount of water passing through the pass during half a period was thus 0.03–0.045 km^3 (or 5–8‰ of the total lagoon volume). Spread over the lagoon, this volume would correspond to a tidal range of 20–35 cm, which is in agreement with our tide observations.

Fig. 5b (bottom panel) shows the residual (i.e. tidally filtered with the Demerliac filter) flow through the pass for the entire period of ADCP measurement. This residual flow was always oriented outward from the lagoon (thus the negative y-axis in Fig. 5b). The mean residual flow over the period was 270 $m^3\ s^{-1}$. It peaked at 470 $m^3\ s^{-1}$ on the 12th of December 2008. Secondary peaks occurred the 17th, 26th of December and again the 4th and 8th of January. Fig. 4a clearly shows that these peaks corresponded either to large waves measured in front of the northern hoa at Station A10 (17th of December) or in front of the southern hoa at Station A02 (26th of December, not shown), or in front of both hoa (12th of December). The highest residual peak corresponds to both hoa being active. Since all the hoa sections summed to 4000 m (split between 500 m in the northern part and 3500 m in the southern part), and considering a mean hoa depth of 50 cm and that the 470 $m^3\ s^{-1}$ of the main peak were uniformly spread among all hoa (supposed active during this event), we obtain an average velocity of 23.5 cm s^{-1} in each hoa. This velocity is consistent with our measured velocities. Moreover, a mean pass outflow of 270 $m^3\ s^{-1}$ led to a 13.5 cm s^{-1} residual velocity in the hoa, close to the value shown Fig. 3b.

Since the model was parameterized with a stable value of hoa current velocity, the model could not reproduce finely in the pass the main peaks, which were thus themselves explained by waves

Table 4
Residual current measured by ADCP under various meteorological conditions at various locations within the lagoon.

Wind conditions/ station	A15	A17	A18
No wind Mean current over the vertical	**Period:** 22/05/2009–26/05/2009 **Mean wind (over the period) at Takaroa station**: 2 m s^{-1}/110° u = 0.0672 m s^{-1} v = −0.0088 m s^{-1} Norm = 0.0678 m s^{-1} Direction = 97.5°	**Period:** 04/08/2009–08/08/2009 **Mean wind (over the period) at Takaroa station**: 2.5 m s^{-1} /170° u = 0.0033 v = −0.0004 Vitesse = 0.0034 Direction = 98.4°	**No available observation**
Trade wind Mean current over the vertical	**Period:** 27/05/2009–06/06/2009 **Mean wind (over the period) at Takaroa station** : 8.5 m s^{-1},114° u = 0.0891 m s^{-1} v = −0.0136 m s^{-1} Vitesse = 0.0901 m s^{-1} Direction = 98.8°	**Period:** 12/09/2009–20/09/2009 **Mean wind (over the period) at Takaroa station**: 7.9 m s^{-1},112° u = 0.0012 m s^{-1} v = −0.0028 m s^{-1} Vitesse = 0.003 m s^{-1} Direction = 149°	**Period:** 03/10/2009–08/10/2009 **Mean wind (over the period) at Takaroa station**: 8.65 m s^{-1},114° u = 0.0343 m s^{-1} v = 0.0188 m s^{-1} Vitesse = 0.0391 m s^{-1} Direction = 55°
Trade wind Current at 2 m below the surface	**Period:** 27/05/2009–06/06/2009 **Mean wind (over the period) at Takaroa station**: 8.5 m s^{-1},114° u = 0.0981 m s^{-1} v = −0.0333 m s^{-1} Vitesse = 0.1036 m s^{-1} Direction = 110°	**Period:** 12/09/2009–20/09/2009 **Mean wind (over the period) at Takaroa station** : 7.9 m s^{-1},112° u = −0.0133 v = −0.0032 Vitesse = 0.0137 Direction = 256°	**Period:** 03/10/2009–08/10/2009 **Mean wind (over the period) at Takaroa station**: 8.65 m s^{-1},114° u = 0.0343 m s^{-1} v = 0.0188 m s^{-1} Vitesse = 0.0391 m s^{-1} Direction = 55°
Trade wind Current at 3 m above the bottom	**Period:** 27/05/2009–06/06/2009 **Mean wind (over the period) at Takaroa station** : 8.5 m s^{-1},114° u = 0.0687 m s^{-1} v = 0.0078 m s^{-1} Vitesse = 0.0691 m s^{-1} Direction = 183°	**Period:** 12/09/2009–20/09/2009 **Mean wind (over the period) at Takaroa station** : 7.9 m s^{-1},112° u = 0.003 m s^{-1} v = 0.00033 m s^{-1} Vitesse = 0.003 m s^{-1} Direction = 84°	**Period:** 03/10/2009–08/10/2009 **Mean wind (over the period) at Takaroa station** : 8.65 m s^{-1},114° u = 0.0343 m s^{-1} v = 0.0188 m s^{-1} Vitesse = 0.0391 m s^{-1} Direction = 55°

forcing hoa currents (see above). Nevertheless, the simulated pass residual flux was oriented outside the lagoon at all times, with an order of magnitude in agreement with observations. Thus, the model reproduced correctly the process of a lagoon filled by hoa and emptied by the pass.

We concluded that the model was able to reproduce correctly the climatological circulation at the lagoon boundary, through the hoa and the pass, with simulations in agreement with measurements, and discrepancies well explained by the parameterization used (with fixed velocities in hoa). The model was then used to investigate the main patterns of the circulation inside the lagoon.

3.4. Residual circulation patterns

Observations suggest that the main driving mechanism of the lagoon circulation that must be accounted for were tide and wind forcing, and not waves, due to the small hoa residual velocities measured year long. For the numerical simulations, tidal conditions were taken realistic whereas the wind forcing was set stationary. The winds observed at the Takaroa meteorological station and considered representative of the synoptic wind were very stable and typical of trade winds. Its interannual mean speed and direction was 8 m s^{-1} and 107°, respectively.

The horizontal residual eulerian currents were properly characterized by the transport or the vertically averaged currents $(\bar{u}, \bar{v})$. It is rather straightforward to see that the transport associated with these currents computed under stationary conditions are divergence-free so that a stream function (ψ) could be derived as : $(h\bar{u}, h\bar{v}) = (-\frac{\partial\psi}{\partial y}, \frac{\partial\psi}{\partial x})$. The isolines of this stream function computed from stationary divergence-free current field coincide with the trajectories of particles that are freely advected in this field. The distance between isolines can be interpreted in terms of flow: the more two isolines are spaced the weaker is the flow passing in between. Thus the isolines reveal neatly the circulation structures, in particular the retention structures which are evidenced as closed circulation cells.

Fig. 6 shows the barotropic current function computed under various stationary meteorological conditions. Fig. 6a shows the transport associated to the tidal circulation only. The pass jet influence was remarkable whereas the transport was very weak elsewhere. The large residual circulation patterns showed that the tidal jet entering through the pass spread preferentially to the east and north-east and went out by pumping water from the south east, giving rise to large cyclonic (or clockwise) circulation patterns. ADCP profiles under weak wind conditions (less than 2 m s^{-1} over 3 days) at point A15 (Fig. 7) showed residual barotropic current in rather good agreement in direction. However; the intensity of the observed current was twice the modeled one. When a climatological wind was activated (Fig. 6b and c), the stream function displayed two main barotropic circulation structures: under climatological trades (6b) a large anticlockwise circulation patterns, located in the north occupied two third of the water body with residual currents of the order of 5 cm s^{-1}. Then, a weaker clockwise circulation patterns appeared in the south. Its shape was strongly constrained by the atoll rim. Two ADCP observations (Table 4) confirmed that in the vicinity of the pass (A15), the residual barotropic current was oriented to the east. Again, measurements showed velocities that double the model prediction. ADCP also confirmed that the residual current in the south (A18) was very weak (<1 cm s^{-1}). Finally, under climatological tradewind conditions, the tidal jet residual influence next to the pass was not visible anymore. It was probably reinforcing the northern circulation cell by spreading to the southeast during flood and pumping from the east-northeast during ebb.

Under western wind conditions (6c) two main spatial patterns emerged. The northern pattern has shifted and flattened along the northern rim and the circulation has been reversed (clockwise). The southern pattern expanded and spread to the east occupying the southern part of the lagoon. Its circulation has also been reversed. In both patterns, the residual currents reached 6 cm s^{-1}. The residual influence of the tidal jet was also modulated by the wind. It seems that it spread along the northern rim and pumped

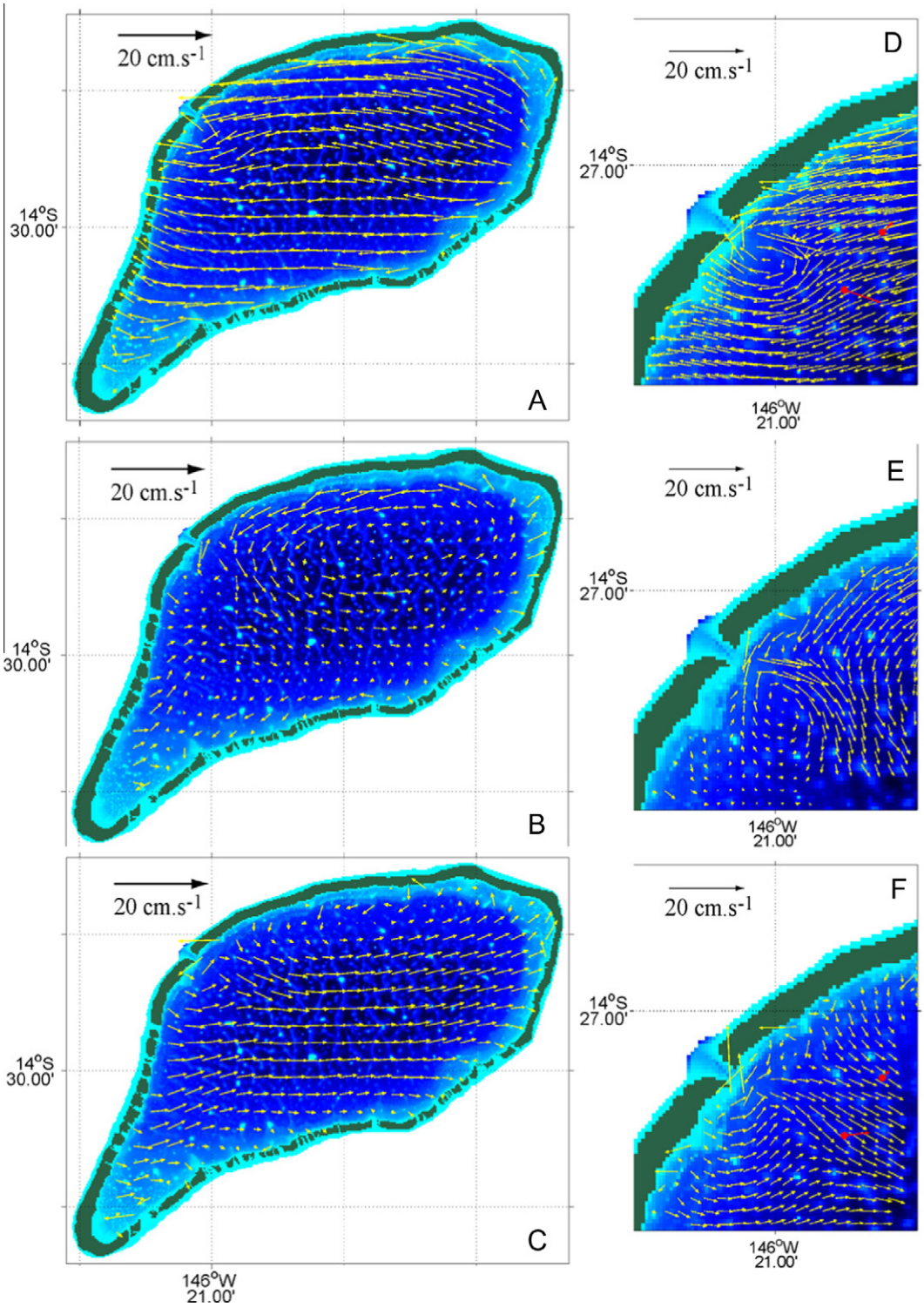

Fig. 8. Modelled residual at 2 m, 15 m below the surface and 2 m above the bottom (A–C). Panels D–F illustrate a zoom on the pass. Arrows show the estimates from ADCP measurements at location A15 and A18.

from the southeast. Everything happened as if the wind forced the shallow parts of the lagoon, inducing currents in the direction of the wind. The deeper part was constrained by continuity, and gave birth to backward currents.

The residual effects of the tidal jet appeared tightly linked to the wind conditions. Indeed, Fig. 7 shows vertical ADCP current profiles recorded at location A15 (22 m deep), in the vicinity of the pass. During this period the wind was first shifting from the north to the southwest. We first noticed the currents variability with respect to time. Currents were below 5 cm s^{-1} from the 10th to 12th of May, with no more tidal cycle visible, except on the direction. Then, the wind returned to a more frequent direction (from the southeast, then to the east). The intensity of the current increased (25 cm s^{-1}) till the end of the period, showing again clear tidal cycles. Attenuation along the vertical due to bottom friction was also noticeable. The direction showed the tidal reverse and most of the

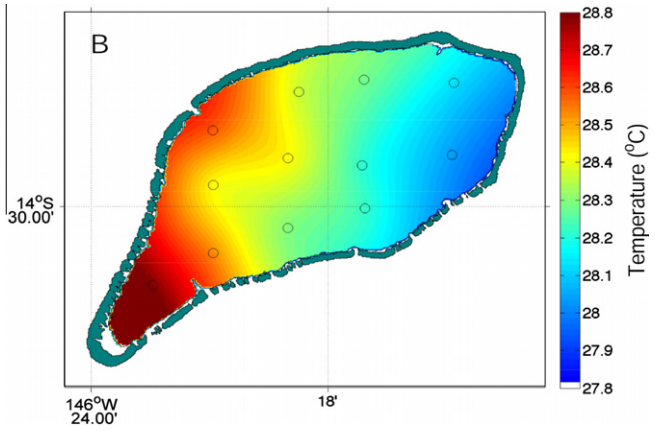

Fig. 9. Sea surface temperature (°C) from CTD casts network achieved the 9th of November 2009. Circles indicate the positions of the 12 measurements, interpolated afterwards.

time the increase of the current modulus from the surface to the bottom, evidencing the bottom Ekman pumping oriented to the right. The surface veering expected to the left at the surface is not seen, likely because an Ekman spiral cannot develop under these conditions. The current reached its maximum on the 21st of May when the wind was blowing again from the east with moderate intensity (6 m s^{-1}).

Last but not least, it clearly appears on Fig. 6a and b that the residual barotropic flow was oriented in the same direction than the wind in the shallow waters whereas it is oriented against the wind in the deeper waters. This can be noticed in both trades and west wind conditions. The Fig. 10 shows that the water column was better mixed in the shallow part of the lagoon. The wind generated current was rather homogeneous along the vertical, giving a vertical averaged current oriented in the direction of the wind on both side of the lagoon. As long as water cannot be accumulated leeward, a return current occurred in the mid part of the basin below the wind generated current.

3.5. The two-layers overturning circulation

Under climatological conditions, the simulated vertical structure circulation yielded a two-layers, overturning, circulation (Fig. 8a and c). The surface currents homogeneously flow downwind at a speed of 10 cm s^{-1}, representing the expected order of magnitude of several percent of wind speed (i.e. 8 m s^{-1}). This downwind layer lies on top of a return layer characterized by currents an order of magnitude slower, typically of few cm s^{-1}. In the middle part (Fig. 8b) of the lagoon, below the Ekman layer (15 m) the barotropic structure seen on Fig. 6a is again noticeable. It also shows that a Ekman spiral could not develop due to the basin shape constraints.

The top layer was about ten meter thick (Fig. 10), which is consistent with the structure showed by Tartinville et al. (1997, Fig. 5) for Mururoa atoll. According to the model, it is thinner in the deeper part of the lagoon. It is thicker in the shallower part, where the bottom mixed layer probably merge with the surface one, mixing the water column.

In the vicinity of the pass (Fig. 8d–f) the flow was the most complex. At the surface, the tidal jet counteracts the effect of the wind (Fig. 8d). The ADCP measurements below the surface at location A15 and A18 2 m were in rather poor agreement with the model. Below 15 m deep, both intensity and direction were in better agreement (Fig. 8f). Model and data show deep residual currents oriented against the wind direction.

The overturning circulation was confirmed by hydrological observations. Fig. 9 shows sea surface temperature (SST) horizontal distribution for the 9th of November 2009, according to CTD casts performed on the L01 to L12 hydrological network stations (Fig. 1b). Wind conditions were close to climatology conditions. For that day, data revealed a clear lagoon-wide thermal stratification which lasted over a week. The SST structure confirmed the circulation structure, with cold waters being upwelled windward along the east side of the rim, and warmer waters being pushed downwind in the southwestern corner of the lagoon.

3.6. The e-flushing time

The eulerian residual currents structure analysis from the previous section does not yield in a straightforward way a view of residence time, since the turbulent fluxes are not accounted for. This point was also discussed by Tartinville et al. (1997). We confirm their conclusions achieved on Mururoa atoll that the large lagoon horizontal gyres seen on the transport stream function tend to trap water parcels, and increase the residence time. This assumption was confirmed here by the computation of the e-flushing time. Fig. 11a shows this e-flushing time computed under typical climatological trade winds. The patterns fit very well with the structure

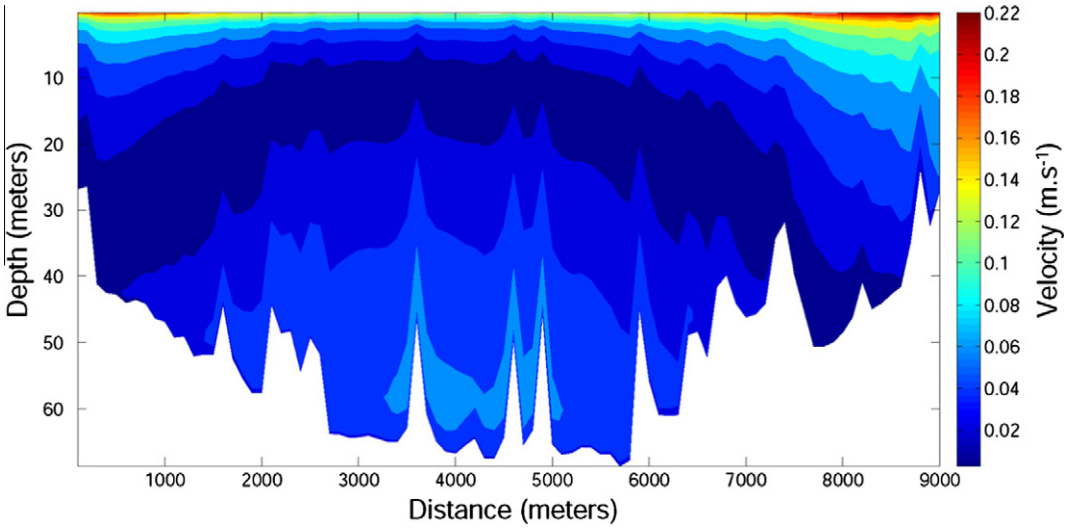

Fig. 10. Middle lagoon (146°18′W) north–south vertical section of the residual currents modelled under stationary trade winds (in m s^{-1}).

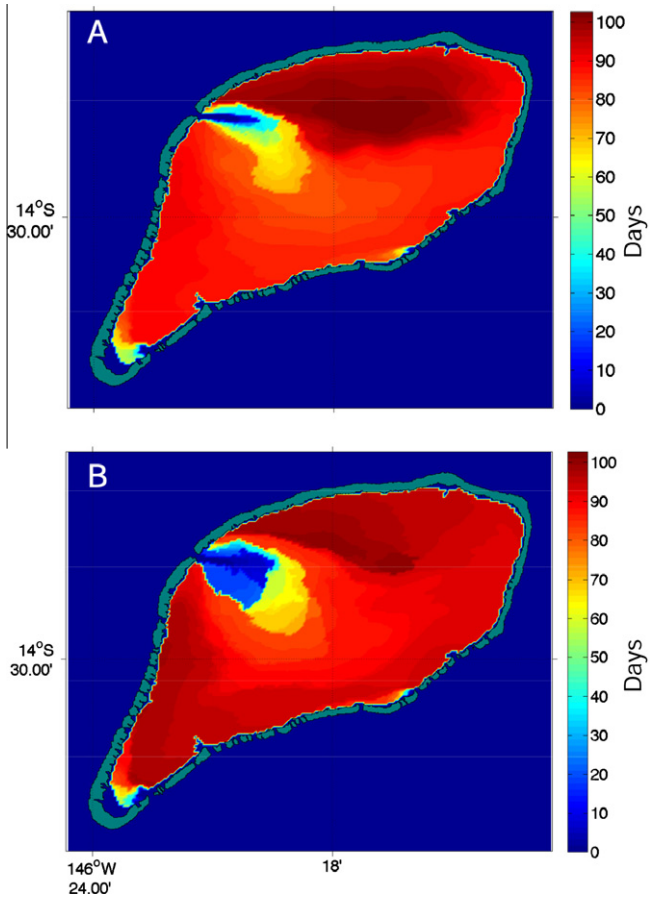

Fig. 11. (a) Resulting e-flushing time under stationary trade winds (107° – 8 m s^{-1}). (b) e-flushing time under realistic winds measured from January to April 2009.

of the stream function (Fig. 6b). The northern gyre shown previously coincided here with a trapped water mass with a e-flushing time greater than 100 days. The pass played a significant role in separating the lagoon into three water-bodies. In the vicinity of the pass, the e-flushing time was lower, about 50–60 days. To the north and to the south, e-flushing times were larger, around 80 days to the south, more than 100 days to the north, and reached 140 days in the core of the northern circulation cell. Furthermore, this structure was rather homogeneous along the vertical (not shown), fitting well with the stream function structure. This is in agreement with the fact that the shorter time scale of the flow is associated with vertical diffusion. The average e-flushing time over the entire domain was about 80 days.

Fig. 11b shows the same quantity computed under a realistic sequence of winds taken from the beginning of January 2009–April 2009. The orders of magnitude were about the same and the structures were similar to the climatological conditions patterns. Nevertheless some differences can be pointed out:

- The influence of the pass was larger towards the south.
- The extension of the north cell was reduced but its e-flushing time remained similar (above 100 days).
- The south cell was clearly reinforced. Its water body seemed to be more isolated, and its e-flushing increased to up to 90 days.

The e-flushing time could be averaged over the entire lagoon during the realistic wind conditions. We obtained a result close to the climatological situation, with an average of 80 days.

4. Discussion

4.1. Residence time, renewal time and e-flushing time

Residence time is a key variable to characterize a water body. Different computation schemes have been proposed (see Jouon et al., 2006 for review), and we have defined here the e-flushing time. Previous studies (Atkinson et al., 1981, Delesalle and Sournia 1992, Tartinville et al., 1997; Kraines et al., 1999; Andréfouët et al., 2001) offered lagoon-scale measurements, typically by establishing a budget between water inputs and outputs at the lagoon boundary, or if spatial numerical methods were involved, they computed the average time needed for a tracked particle to leave the lagoon. The power of a well validated, trustable, numerical 3D model is of course to provide a spatially-explicit view (a map) of the variations of residence time in the focal lagoon, itself leading to an integrated lagoon-scale water renewal time when needed (Andréfouët et al., 2001). For Ahe lagoon, if we consider the average output residual flux through the main pass estimated by the ADCP measurements and if we assume that all the water entering through the hoa is eventually flushed out by the pass, then the water body is renewed at the rate of this flow. This was estimated at around 260 m^3 s^{-1}, which for a 5.9 km^3 lagoon volume, yields a renewal time of 252 days. This renewal time is not what is observed in the computed e-flushing time (Fig. 11). Indeed, the model accounts for the spatial structure of the circulation and specifically for the action of the tidal flow through the pass. As demonstrated in the previous sections, the pass partitions the lagoon into three circulation cells. Inbound flows entering the lagoon through the southern rim does not flow homogenously and directly to the pass. This flow is trapped in the various cells of circulation where the e-flushing time is above 80 days almost everywhere except in the vicinity of the pass.

In terms of larval dispersal and spat collecting, the e-flushing time is relevant assuming there is a synchronous and homogeneous spawning at the initial time, over the entire domain. Illustrations of the spatial variations in terms of retention, accumulation and exports are provided by Thomas et al. (2012a,b) who complete the picture given here.

4.2. Tide-driven lagoon flushing and circulation

The lagoon water flushing through the pass influences primarily the lagoonal volume next to the pass (Fig. 11). The net flushing is significant, under the assumption that the water mass re-entering the lagoon is not the same than the water that just left. This process could rapidly renew the water body even if the residual flow of this purely tidal-driven process is quantitatively null. Under the above assumption, the Ahe model suggests that tidal flushing decreases the renewal time: the mean e-flushing – which could be considered of the same order of magnitude as the renewal – time is around 80 days whereas the renewal time is of 252 days. This is in contrast with Callaghan et al. (2006) who concluded that wave flushing was more efficient than pure tidal flushing. Of course atolls studied by Callaghan et al. (2006) did not have a pass, had larger reef flat width to perimeter ratios, and likely had a different, more energetic, wave climate. We conclude here for Ahe that tide is the major flushing driver as long as it is combined to wind forcing. In fact, the internal circulation induced by tide alone (Fig. 6a) is very weak and yields lagoon scale renewal time and average e-flushing time far longer than those obtained when the wind is blowing. Tartinville et al. (1997) made similar observations for Mururoa atoll, although Kraines et al. (1999) insisted that in Majuro Atoll, the main flushing driver was the radiation-stress-driven flow (i.e. wave flushing) from the reef flats through the hoa.

4.3. Overturning circulation and stratification

CTD casts have been performed in Ahe atoll lagoon in 2008–2009 during surveys aimed at characterizing relationships between pearl oyster larvae densities and hydrological conditions (Thomas et al., 2012a,b). The same L02-L12 stations were used here to compute a mean average stratification presented on Fig. 12. Fig. 12 confirms a frequent detectable stratification occurring in Ahe lagoon, with surface and bottom SST differences in 2008 and 2009, depending on wind speed (averaged here over the 3 days preceding the observations). The wind component the most correlated with the stratifications is the one projected on the 35° axis of the lagoon, in other words parallel the largest atoll dimension. However, most of the time the thermal stratification is very weak: in 80% of the observed situations, they are below 0.3 °C. It is also noticeable that negative thermal stratifications (i.e. bottom temperature higher than surface temperature) frequently occurs and seems to be compensated by negative haline stratification.

With winds blowing above 3 m s^{-1} in the 35° direction, the stratifications are very weak (less than 0.2 °C), whereas in light to medium wind conditions, the lagoon waters may get stratified. Observed stratification frequently reach above 0.4 °C, and up to 1.2 °C (in November 2009). Typically, under such thermal flux and wind conditions, the water column is stratified. This is seen oceanward just outside the lagoon on CTD casts performed at the same time. Casts showed a sharp thermocline located at 45 m. Thermal stratification appeared much more limited in the lagoon. The de-stratification cannot be explained easily by direct mixing due to wind, neither because of bottom friction generated turbulence, since bottom currents remained very weak. The general overturning circulation is likely to be responsible for the mixing of the lagoon water body. In light to medium wind conditions, the overturning circulation weakens, allowing the development of a vertical stratification. In more intense wind, the circulation is strong enough to prevent stratification, by upwelling windward the bottom cold water and downwelling leeward the surface warm water. This explanation is confirmed by the weak stratifications observed under light wind conditions. This probably shows that wind direction rather than wind intensity make the overturning circulation more or less efficient tin mixing the water column. The most intense stratification over the 3 years (2007–2009) was observed during period of wind coming from 130° (November 8–10th 2009), a direction which significantly departs from the climatological tradewinds (i.e. 107°). Nevertheless, the stratification in Ahe appear limited in intensity and in time. This could explain why stratification was neither reported by Atkinson et al. (1981) in Enewetak nor Kraines et al. (1999) in Majuro, although it may occur in Ahe.

4.4. Comparing atoll lagoons hydrodynamics: towards a functional typology of Pacific Ocean atolls?

Following Atkinson et al. (1981), Ahe atoll lagoon can be classified as a "deep" lagoon not only because of its average depth but in the sense that circulation is dominated by wind and not by tide, and because the primary wind-driven circulation pattern is a downwind surface flow and a returning upwind deep flow. However, Ahe lagoon departs from the circulation scheme described by Atkinson et al. (1981) for Enewetak lagoon in the Marshall Islands, and by von Arx (1948) for Bikini lagoon, also in the Marshall Islands. In Enewetak, radiation stress due to breaking waves on the windward eastern side are an important forcing factors of water exchanges and circulation, but not in Ahe. The geomorphology of the atolls are also very different with three passes in Enewetak, each with their own behaviour, *versus* one in Ahe. These passes oriented the deep water flows in Enewetak, but not in Ahe. Moreover, in terms of water exchanges, whereas Atkinson et al. (1981) reported a net positive (albeit weak) outflow across the Enewetak leeward rim margin, in Ahe, the entire windward wave-driven flow was flushed through the pass. Indeed, if we consider at Ahe that the average speed within the hoa are of the order of 10 cm s^{-1} as observed, this yields a total windward flux (assuming that all the southern hoa work in the same way) of the order of 260 m^3 s^{-1}. On the leeward side, the maximum speed observed was around 20 cm s^{-1} giving a total output flux of 30 m^3 s^{-1}. In the same time, the mean output flux in the main pass was around 260 m^3 s^{-1}. The conclusion is that the lagoon water body received water windward but flushed entirely this excess water through the main pass.

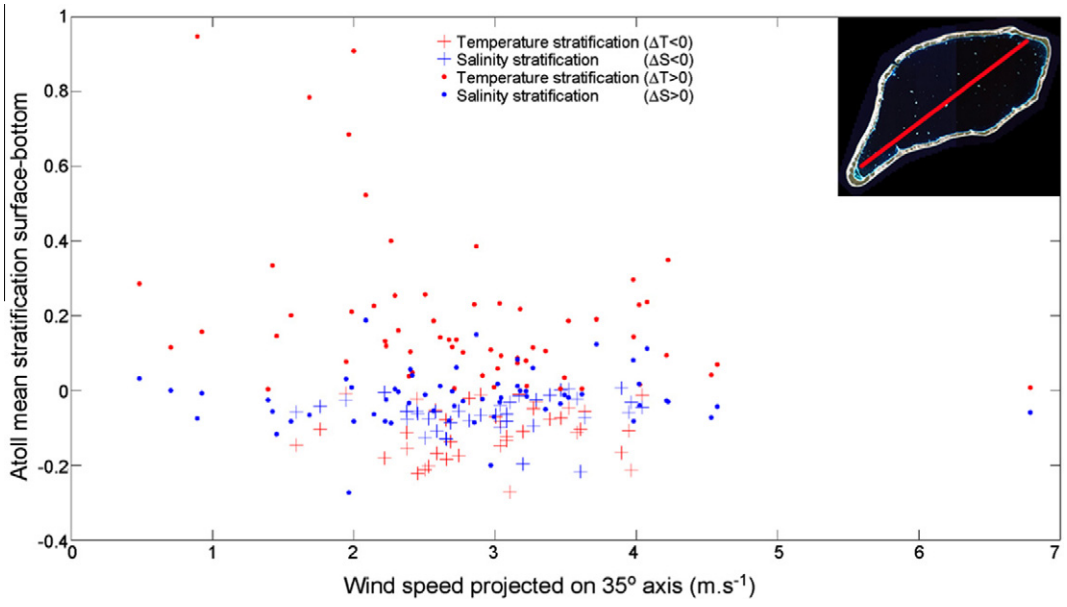

Fig. 12. Mean thermal and haline stratifications (surface minus bottom) computed over the eleven stations of the CTD observation network. Red dots are positive thermal stratifications, blue dots are haline stratification. Same for the crosses that show negative thermal stratification. The *x*-axis is the average wind over the past 3 days projected on the 35° axis (largest dimension) of the lagoon. (For interpretation of the references to colour in this figure legend, the reader is referred to the web version of this article.)

The circulation patterns and computed time scales in Ahe appear very close to Mururoa's (Tartinville et al., 1997) despite the different morphology (5 km wide pass, 33 mean depth in Mururoa *versus* a 0.2 km wide pass and 41 m mean depth in Ahe). Hoa played a minor role in both atolls. Typical velocity observed in the hoa were weak (around 10 cm s^{-1} and in case of Ahe peaking at 35 cm s^{-1}) (Tartinville and Rancher, 2000) and their depth and cumulated length were small compared to the perimeter of the rim. Thus, most aspects of the circulation were driven by wind and tide, justifying their classifications as "Deep" lagoons (Atkinson et al., 1981). However, the rim geomorphology plays a significant role and influence the circulation in the lagoons: in Ahe, the pass divided the circulation inside the lagoon into three main cells whereas the 5 km-long pass in Mururoa confined only a single cell along the southern rim. Barotropic transport was weaker in Ahe, with the stream function peaking at 300 $m^3 s^{-1}$ in Ahe *versus* 1500 $m^3 s^{-1}$ in Mururoa under the same wind forcing (i.e. about 8 m s^{-1}). Renewal times obtained with comparable methods were of comparable magnitude with 80 and 100 days in Ahe and Mururoa, respectively.

Despite the differences primarily explained by a semi-closed geomorphology, Ahe atoll shares several general circulation features with previously describe Pacific open atolls, such as Bikini (von Arx, 1948), Enewatak (Atkinson et al., 1981), Mururoa (Tartinville et al., 1997) and Majuro (Kraines et al., 1999). The vertical structure circulation that we obtain by simulation in Ahe lagoon has already been described for Bikini, Enewatak and Mururoa. In contrast, for atolls without passes, excess waters due to wave radiation stress cannot be flushed through these passes. Instead, flushing occurs by gravity when the lagoon surface reaches an elevation allowing water to flow oceanward across the rim located on the protected side of the atoll, from the opposite direction of the incident waves. The hydrodynamic functioning of such a closed atoll (in the sense that there is no pass) has been formalized by Callaghan et al. (2006) for two Cook Islands atolls (Manihiki and Rakahanga). They described a flushing mechanism driven by wave pumping on the exposed side of the rim and modulated by the ocean tide. A key feature is that lagoon water levels remain above the ocean level regardless of the tidal phase.

5. Conclusion

If we consider the small completely closed atolls (no pass, neither any functional reef flats, such as Taiaro and Clipperton, in Leclerc et al. (1999) and Charpy et al. (2010)), the small atolls with no passes but with reef flats (Manihiki and Rakahanga studied by Callaghan et al. (2006)), the small open but deep and compartmentalized atoll (Palmyra, Gardner et al., 2011), the large open atolls with passes and reef flats (Enewetak, Bikini, Majuro, Mururoa studied by authors cited above), the case study represented by Ahe atoll (medium size, deep atoll, semi-closed with passes and few reef flats) offers a different geomorphological setting, and not surprisingly a somewhat different scheme and set of conclusions compared to all the previous studies.

Among the studied Pacific atolls, only Majuro, Mururoa, Ahe and Takaroa (unpublished results, but similar study as Ahe presented here) lagoons have been studied with 3D numerical models to our knowledge (Andréfouët et al., 2006). Other atolls have been characterized from *in situ* physical and hydrobiological measurements only but they equally contribute to establish the continuum of variations in atoll hydrodynamics functioning. Since there are no large, closed atolls in the Pacific Ocean (nor elsewhere), the geomorphological range of studied atolls is now getting significant and quite complete. Establishing a hydrodynamical typology of lagoons based only on geomorphology would be a first logical step, but each atoll needs to be related to its physical boundary conditions to be rigorous and before generalizing. A previous atoll classification based on water renewal time was established for Tuamotu Archipelago according to geomorphology and wave forcing (Andréfouët et al., 2001). Wave forcing is a critical parameter that can vary widely between atolls at short distance. For instance, Ahe and Takaroa atolls wave climate is quite different than atolls only 100 km away due to the sheltering barrier-effects of large atolls in the south (Andréfouët et al., 2012b). Lagoon-scale variables were used for this previous Tuamotu atoll classification, but an atoll typology based on the relative importance of the wind-driven, tide-driven, wave-driven, and density-driven processes on the internal lagoon circulation is now shaping up.

In terms of aquaculture, the results obtained here highlight the weak flushing of Ahe lagoon that itself leads to renewal time and e-flushing time that appear very long (at least some tenths of days) compared to the larval life of the pearl oyster *P. margaritifera* (15–30 days, Thomas et al., 2012a,b). Thus, the retention capability of Ahe appears very interesting in regards to larval dispersal and the potential for spat collecting, contributing to explain analytically why Ahe is one of the most important producers of pearl oyster juveniles in French Polynesia.

Finally, the 3D model of Ahe lagoon will provide the needed diagnostic tool to characterize the physical mechanisms that control the spatio-temporal variations of biological variables in the water column, such as planktonic communities.

Acknowledgements

This study was funded by the 9th European Development Fund (Grant POF/001/002N°1 to Serge Andréfouët and Loic Charpy, IRD) through the French Polynesia Service de la Perliculture. The authors are grateful to the colleagues who participated to the numerous surveys and to the project in general, specifically Alain Loyat (Project manager), Joël Orempuller, Nicolas Maihota, Jean-Yves Panché, David Varillon, Francis Gallois, Mainui Tanetoa, and Nahiti Vernaudon, from IRD-Tahiti, IRD US191 in Nouméa and Service de la Perliculture. Useful insights were provided by Sylvain Ouillon and Pascal Douillet in the early stages of the project. Météo France and the French Hydrographic Service provided data for this study. GéoPolynésie (Christian Friot) was contracted for the bathymetry survey of Ahe atoll.

References

Andréfouët, S., Pagès, J., Tartinville, B., 2001. Water renewal time for classification of atoll lagoons in the Tuamotu Archipelago (French Polynesia). Coral Reefs 20, 399–408.

Andréfouët, S., Ouillon, S., Brinkman, R., Falter, J., Douillet, P., Wolk, F., Smith, R., Garen, P., Martinez, E., Laurent, V., Lo, C., Remoissenet, G., Scourzic, B., Gilbert, A., Deleersnijder, E., Steinberg, C., Choukroun, S., Buestel, D., 2006. Review of solutions for 3D hydrodynamic modeling applied to aquaculture in South Pacific atoll lagoons. Marine Pollution Bulletin 52, 1138–1155.

Andréfouët, S., Charpy, L., Lo-Yat, A., Lo, C., 2012a. Recent research for pearl oyster aquaculture management in French Polynesia. Marine Pollution Bulletin 65, 407–414.

Andréfouët, S., Ardhuin, F., Quefeullou, P., Le Gendre, R., 2012b. Island shadow effects and the wave climate of the Western Tuamotu Archipelago (French Polynesia) inferred from altimetry and numerical model data. 65, 415–424.

Atkinson, M., Smith, S.V., Stroup, E.D., 1981. Circulation in Enewetak atoll lagoon. Limnology and Oceanography 26, 1074–1083.

Blumberg, A. F. and G. L. Mellor (1987). A description of a three-dimensional coastal ocean circulation model, Three-Dimensional Coastal ocean Models, edited by N. Heaps, 208 pp., American Geophysical Union, 1987.

Callaghan, D., Nielsen, P., Cartwright, N., Gourlay, M., Baldock, T., 2006. Atoll lagoon flushing forced by waves. Coastal Engineering 53, 691–704.

Charpy, L., Rodier, M., Couté, A., Perrette-Gallet, C., Bley-Loëz, C., 2010. Clipperton, a possible future for atoll lagoons. Coral Reefs 29, 771–783.

Delesalle, B., Sournia, A., 1992. Residence time of water and phytoplankton biomass in a coral reef lagoons. Continental Shelf Research 12, 939–949.

Demerliac, A., 1974. Calcul du niveau moyen journalier de la mer. Rapport du service hydrographique de la marine 741, 49–57.

Dufour, P., Andréfouët, S., Charpy, L., Garcia, N., 2001. Atoll morphometry controls lagoon nutrient regime. Limnology and Oceanography 46, 456–461.
Gardner, J.P.A., Garton, D.W., Collen, J.D., 2011. Near-surface mixing and pronounced deep-water stratification in a compartmentalised, human-disturbed atoll lagoon system. Coral Reefs 30, 271–282.
Gaspar, P., Grégoris, Y., Lefevre, J., 1990. A simple eddy kinetic energy model for simulations of the oceanic vertical mixing: tests at Station Papa and long-term upper ocean study site. Journal of Geophysical Research 95 (C9), 179–193.
Jouon, A., Douillet, P., Ouillon, S., Fraunié, P., 2006. Calculations of hydrodynamic time parameters in a semi-opened coastal zone using a 3D hydrodynamic model. Continental Shelf Research 26, 1395–1415.
Kraines, S., Suzuki, A., Yanagi, T., Isobe, M., Guo, X., Komiyama, H., 1999. Rapid water exchange between the lagoon and the open ocean at Majuro Atoll due to wind, waves, and tide. Journal of Geophysical Research 104 (C7), 15635–15653.
Lazure, P., Dumas, F., 2008. An external-internal mode coupling for a 3D hydrodynamical model for applications at regional scale (MARS). Advances in Water Resources 31, 233–250.
Leclerc, A.M., Baptiste, P., Texier, D., Broc, D., 1999. Density induced water circulation in atoll coral reefs: a numerical study. Limnology and Oceanography 44, 1268–1281.
Luyten, P.J., De Mulder, T., 1992. A module representative surface fluxes of momentum and heat. Technical report No. 9 MAST-0050-C (Mumm), 30pp.
Lyard, F., Lefevre, F., Letellier, T., Francis, O., 2006. Modelling the global ocean tides: modern insights from FES2004. Ocean Dynamics 56, 394–415.
Pawlowicz, R., Beardsley, B., Lentz, S., 2002. Classical tidal harmonic analysis including error estimates in MATLAB using T_TIDE. Computers and Geosciences 28, 929–937.
Pugh, D.T., 1979. Sea levels at Aldabara atoll, Mombasa and Mahé, western equatorial Indian Ocean, related to tides, meteorology and ocean circulation. Deep Sea Research 26, 237–258.
Salvat, B., 2009. Dominant benthic mollusks in closed atolls, French Polynesia. Galaxea 11, 197–206.
Tartinville, B., Rancher, J., 2000. Wave-induced flow over Mururoa atoll reef. Journal of Coastal Research 16, 776–781.
Tartinville, B., Deleersnijder, E., Rancher, J., 1997. The water residence time in the Mururoa atoll lagoon: sensitivity analysis of a three-dimensional model. Coral Reefs 16, 193–203.
Thomas, Y., Le Gendre, R., Garen, P., Dumas, F., Andréfouët, S., 2012a. Bivalve larvae transport and connectivity within the Ahe atoll lagoon (Tuamotu Archipelago), with application to pearl oyster aquaculture management. Marine Pollution Bulletin 65, 441–452.
Thomas, Y., Garen, P., Bennett, A., Le Pennec, M., Clavier, J., 2012b. Multi-scale disctribution and dynamics of bivalve larvae in a deep atoll lagoon (Ahe, French Polynesia). Marine Pollution Bulletin. 65, 453–462.
Von Arx, W.S., 1948. The circulation systems of Bikini and Rongelap lagoons. Transactions, American Geophysical Union 29, 861–870.